

# EFFICIENT IMPLEMENTATION OF THE PROJECTION OPERATOR IMAGINARY TIME SPECTRAL EVOLUTION (POITSE) METHOD FOR EXCITED STATES

PATRICK HUANG, ALEXANDRA VIEL, AND K. BIRGITTA WHALEY

*Department of Chemistry and Kenneth S. Pitzer Center for Theoretical Chemistry,  
University of California, Berkeley, CA 94720-1460, USA*

We describe and systematically analyze new implementations of the Projection Operator Imaginary Time Spectral Evolution (POITSE) method for the Monte Carlo evaluation of excited state energies. The POITSE method involves the computation of a correlation function in imaginary time. Decay of this function contains information about excitation energies, which can be extracted by a spectral transform. By incorporating branching processes in the Monte Carlo propagation, we compute these correlation functions with significantly reduced statistical noise. Our approach allows for the stable evaluation of small energy differences in situations where the previous POITSE implementation was limited by this noise.

## 1 Introduction

The Projection Operator Imaginary Time Spectral Evolution (POITSE) method has allowed calculation of excited states to be made with diffusion Monte Carlo (DMC) without nodal constraints.<sup>1</sup> The main requirement is that a reasonable ground state wave function be available, which can be obtained from well-established ground state methods such as DMC. The excited states are then accessed via projector operators, whose evolution in imaginary time contain information on excited state energies. In the POITSE method a correlation function of the projection operators is evaluated by Monte Carlo techniques, and then subsequently inverted to obtain spectral functions whose peak positions correspond to excited state energies. This inversion requires an inverse Laplace transform, a notoriously ill-conditioned numerical procedure. In the applications of POITSE made to date,<sup>2,3,4</sup> this inversion has been performed with the Maximum Entropy Method (MEM).<sup>5</sup> POITSE has considerable power in allowing analysis of excited states without imposing nodal restrictions. It is particularly useful when some physical insight about the nature of the desired excited states is available. This information can be used to tailor suitable projectors to obtain maximum overlap with the eigenstates of interest. This has been demonstrated recently with permutation symme-

---

Reprinted from P. Huang, A. Viel, and K. B. Whaley, in *Recent Advances in Quantum Monte Carlo Methods, Part II*, edited by W. A. Lester, Jr., S. M. Rothstein, and S. Tanaka (World Scientific, Singapore, 2002), p. 111.

try tunneling excitations.<sup>4</sup> In general, the viability and power of the method has now been shown for a range of model systems involving atomic motions.<sup>2</sup> It has been applied to several physical examples of cluster excitations which cannot be addressed by basis set methods, including up to 15-dimensional problems.<sup>3</sup> To our knowledge, the method has not yet been systematically applied to fermion problems, although there is no intrinsic impediment to this.

In this paper we analyze the efficiency and accuracy of the POITSE algorithm for various different implementations of the DMC component of the method. We present a modification of the algorithm that allows the calculation of small energy differences with reduced statistical noise. In Sec. 2, we briefly review the POITSE general formalism and explain in detail the different numerical implementations. Sec. 3 illustrates the different implementations with two applications: the one-dimensional problem of the ammonia inversion mode and the six-dimensional van der Waals vibration of the <sup>4</sup>He-benzene dimer.

## 2 Computational Methodology

The general POITSE method involves the Monte Carlo evaluation of an imaginary time ( $\tau = it$ ) correlation function  $\tilde{\kappa}(\tau)$ , and then a subsequent inverse Laplace transform of this correlation function using the Maximum Entropy Method. With an appropriately chosen correlation function, the inverse Laplace transform provides a spectral function whose peak positions correspond to excitation energies. The basic theory<sup>1</sup> and its application to model systems<sup>2,3,4</sup> have previously been described in detail, and thus we will only present a brief summary of the relevant formalism.

### 2.1 Theory

The primary quantity of interest in POITSE is the spectral function  $\kappa(E)$ ,

$$\kappa(E) = \sum_n |\langle \phi_0 | \hat{A} | \phi_n \rangle|^2 \delta(E - E_n + E_0), \quad (1)$$

where  $\{|\phi_n\rangle\}$  and  $\{E_n\}$  are a complete set of energy eigenkets and eigenenergies for the Hamiltonian  $\hat{H}$ , and  $\hat{A}$  is an operator chosen to connect  $|\phi_0\rangle$  at least approximately to the particular excited state(s) of interest  $|\phi_n\rangle$ . Taking the Laplace transform of Eq. (1), one can obtain the imaginary time correlation function  $\tilde{\kappa}(\tau)$ , in atomic units ( $\hbar = 1$ ), as

$$\tilde{\kappa}(\tau) = \langle \phi_0 | \hat{A} e^{-(\hat{H} - E_0)\tau} \hat{A}^\dagger | \phi_0 \rangle \quad (2)$$

$$= \sum_n |\langle \phi_0 | \hat{A} | \phi_n \rangle|^2 e^{-(E_n - E_0)\tau}. \quad (3)$$

The POITSE approach consists of evaluating  $\tilde{\kappa}(\tau)$  by a Monte Carlo algorithm, then taking its inverse Laplace transform to obtain the spectral function  $\kappa(E)$ .

In most situations, however, the ground state  $|\phi_0\rangle$  is not known exactly. In practice, one typically employs a trial function  $|\Psi_T\rangle$  and reference energy  $E_{ref}$  which approximate as closely as possible  $|\phi_0\rangle$  and  $E_0$ , respectively. Use of a reference energy not equal to the exact ground state energy modifies the decay rate of all terms in Eq. (3) by a constant factor of  $E_{ref} - E_0$ . This results in a systematic bias in the excitation energies of Eq. (1), independent of the usual finite time step bias due to the DMC evaluation of Eq. (3). This bias from  $E_{ref}$  is also independent of whether the true ground state  $|\phi_0\rangle$  is used.

It has been shown earlier<sup>1</sup> that such systematic bias can be eliminated by introducing the normalization factor

$$\langle \Psi_T | e^{-(\hat{H} - E_{ref})\tau} | \Psi_T \rangle. \quad (4)$$

The removal of bias due to  $E_{ref}$  can be seen from the following arguments. First, replacing  $|\phi_0\rangle, E_0$  in Eq. (2) with  $|\Psi_T\rangle, E_{ref}$ , respectively, and dividing by the additional normalization factor of Eq. (4), leads to the modified decay function

$$\tilde{\kappa}(\tau) = \frac{\langle \Psi_T | \hat{A} e^{-(\hat{H} - E_{ref})\tau} \hat{A}^\dagger | \Psi_T \rangle}{\langle \Psi_T | e^{-(\hat{H} - E_{ref})\tau} | \Psi_T \rangle}. \quad (5)$$

$|\Psi_T\rangle$  is then expanded in eigenstates of  $\hat{H}$  to yield<sup>1,6</sup>

$$\tilde{\kappa}(\tau) = \frac{\sum_n |\langle \Psi_T | \hat{A} | \phi_n \rangle|^2 e^{-(E_n - E_{ref})\tau}}{\sum_m c_m^2 e^{-(E_m - E_{ref})\tau}}, \quad (6)$$

where  $c_m = \langle \Psi_T | \phi_m \rangle$ . The numerator and denominator of Eq. (6) may then be multiplied by  $e^{(E_0 - E_{ref})\tau} / c_0^2$  to obtain

$$\tilde{\kappa}(\tau) = \left[ 1 + \sum_{m=1} \left( \frac{c_m}{c_0} \right)^2 e^{-(E_m - E_0)\tau} \right]^{-1} \sum_n \left| \frac{\langle \Psi_T | \hat{A} | \phi_n \rangle}{\langle \Psi_T | \phi_0 \rangle} \right|^2 e^{-(E_n - E_0)\tau} \quad (7)$$

$$\propto \sum_n |\langle \Psi_T | \hat{A} | \phi_n \rangle|^2 e^{-(E_n - E_0)\tau} + O(x). \quad (8)$$

Here, the prefactor of Eq. (7) was expanded in a power series in  $x$ , where

$$x = \sum_{m=1} \left( \frac{c_m}{c_0} \right)^2 e^{-(E_m - E_0)\tau}. \quad (9)$$

When  $|\Psi_T\rangle = |\phi_0\rangle$ , we see that Eq. (8) is identically equal to Eq. (3), and the effects of using a reference energy other than the true ground state energy are completely eliminated. Additive errors of  $O(x)$  and higher are present when an approximate ground state is used. Note that since the series expansion of Eq. (7) is only convergent for  $c_0 > \sqrt{\frac{1}{2}}$ , this does require that a reasonable approximation to the ground state be available. The higher order terms  $O(x)$  contribute to the spectral function  $\kappa(E)$  in an additive manner. Consequently, they do not affect the positions of the relevant spectral features of interest, *i.e.* the dominant leading terms of Eq. (8). In practice, for a reasonable choice of  $|\Psi_T\rangle$  these additional terms have highly reduced weight.<sup>1,6</sup> To leading order therefore, the renormalized decay Eq. (5) exhibits the time dependence of Eq. (3), independent of the reference energy  $E_{ref}$ . Consequently  $E_{ref}$  may be arbitrarily chosen and varied. The usefulness of this will become more apparent below, in our discussion of numerical implementation.

The numerical inversion of  $\tilde{\kappa}(\tau)$  to obtain  $\kappa(E)$  is an ill-conditioned problem, especially when Monte Carlo noise is non-negligible and/or when the spectral function  $\kappa(E)$  contains multiple overlapping peaks of comparable intensity. Thus a judicious choice of the operator  $\hat{A}$  is necessary to ensure that the time-dependence of  $\tilde{\kappa}(\tau)$  is dominated by only one or a few well-separated energy differences. The inverse Laplace transform of  $\tilde{\kappa}(\tau)$  is performed using the Bryan implementation<sup>5</sup> of the maximum entropy method. Our use of this approach for the inversion of  $\tilde{\kappa}(\tau)$  is identical to that employed in previous POITSE work.<sup>1,3,4,2</sup> We will discuss choices for  $\hat{A}$  specific to particular systems of study in Sec. 3.

## 2.2 Numerical Implementation

The correlation function of Eq. (5) may be rewritten in a form amenable to Monte Carlo evaluation as<sup>1</sup>

$$\tilde{\kappa}(\tau) = \frac{\sum_j \hat{A}^\dagger(\mathbf{R}_j^{(0)}) \hat{A}(\mathbf{R}_j^{(\tau)}) w(\mathbf{R}_j^{(\tau)})}{\sum_j w(\mathbf{R}_j^{(\tau)})}, \quad (10)$$

where  $\mathbf{R}_j^{(\tau)}$  is a guided random walk  $j$  in multidimensional configuration space, discretized in time steps of size  $\Delta\tau$  (a DMC “walker”), and

$$w(\mathbf{R}_j^{(\tau)}) = \prod_m \exp\{-[E_L(\mathbf{R}_j^{(m\Delta\tau)}) - E_{ref}]\Delta\tau\}, \quad (11)$$

$$E_L(\mathbf{R}_j^{(\tau)}) = \Psi_T^{-1}(\mathbf{R}_j^{(\tau)}) \hat{H} \Psi_T(\mathbf{R}_j^{(\tau)}). \quad (12)$$

The quantities  $w(\mathbf{R}_j^{(\tau)})$  and  $E_L(\mathbf{R}_j^{(\tau)})$  are the usual DMC cumulative weight and local energy, respectively.<sup>7</sup> The evaluation of Eq. (10) begins with a variational Monte Carlo (VMC) walk in which an initial starting ensemble of walkers distributed according to  $\Psi_T^2(\mathbf{R})$  is generated using a simple Metropolis method.<sup>7</sup> The starting VMC ensemble is subsequently propagated in imaginary time by a DMC sidewalk, during which Eq. (10) is sampled. Since the maximum entropy analysis requires independent samples of  $\tilde{\kappa}(\tau)$ , the starting configuration for each DMC sidewalk is taken from the VMC walk every 100 – 200 VMC steps apart, to minimize correlations between successive sidewalks. The set of  $\tilde{\kappa}(\tau)$ 's evaluated in this manner serve as input for the inverse Laplace transform via MEM. Typically 100 – 500 independent decays are required to produce a converged spectrum  $\kappa(E)$ .

In the original implementation of Blume *et al.*,<sup>1</sup> the DMC weights  $w(\mathbf{R}_j^{(\tau)})$  take on a continuous range of values, and walkers are not destroyed or duplicated. We refer to this approach here as DMC with pure weights. This is the preferable implementation in an ideal situation where high-quality trial functions are available. However, for reasonably complex systems this is often not the case. In addition, it has been shown that DMC with pure weights is unstable for long propagation times.<sup>8</sup> Therefore, as we demonstrate in Sec. 3, a DMC sidewalk that uses pure weights may sometimes be impractical in situations involving small energy differences.

A common solution to the problems associated with pure weights is to introduce branching. The simplest branching scheme rounds the walker weight at every step of the walk to an integer  $n_j = \text{int}[w(\mathbf{R}_j^{(\tau)}) + \xi]$ , where  $\xi$  is an uniformly distributed random number on  $[0, 1)$ . A walker  $\mathbf{R}_j^{(\tau)}$  is destroyed for  $n_j = 0$ ; otherwise,  $n_j$  copies of walker  $\mathbf{R}_j^{(\tau)}$  are propagated independently in the next DMC move. In this case, the weights  $w(\mathbf{R}_j^{(\tau)})$  take on only integer values, and Eq. (10) becomes

$$\tilde{\kappa}(\tau) = \frac{1}{n_w} \sum_{j'}^{n_w} \hat{A}^\dagger(\mathbf{R}_j^{(0)}) \hat{A}(\mathbf{R}_{j'}^{(\tau)}), \quad (13)$$

where the index  $j$  denotes the parent walker at initial time  $\tau = 0$  from which walker  $j'$  at time  $\tau$  descended, and the instantaneous ensemble size  $n_w$  fluctuates with time. We refer to this approach here as DMC with pure branching. While the pure branching method is formally correct on average and is much more stable numerically, the integer rounding of walker weights can nevertheless lead to greater statistical noise.<sup>9</sup>

To minimize this noise, one can employ a hybrid approach where each

weight  $w(\mathbf{R}_j^{(\tau)})$  is allowed to vary continuously, and a walker is only destroyed or duplicated when its weight exceeds some predetermined bounds. In such a situation, it is important that the branching procedure does not artificially alter the ensemble sum of weights  $W_{tot} = \sum_j w(\mathbf{R}_j^{(\tau)})$ . A combined weighting and branching scheme will in general exhibit less statistical noise than a pure branching scheme. In some cases the noise reduction can be significant. Our implementation of branching is similar to that outlined in Ref. 10. About every 20 – 50 DMC time steps, the ensemble is checked for walkers whose weight exceeds the empirically determined bounds  $w_{min}$  and  $w_{max}$ . A walker  $\mathbf{R}_j^{(\tau)}$  with weight  $w(\mathbf{R}_j^{(\tau)}) > w_{max}$  is split into  $n_j = \text{int}[w(\mathbf{R}_j^{(\tau)}) + \xi]$  walkers, each with weight  $w(\mathbf{R}_j^{(\tau)})/n_j$ . A walker  $\mathbf{R}_j^{(\tau)}$  with weight  $w(\mathbf{R}_j^{(\tau)}) < w_{min}$  is either a) killed with probability  $1 - w(\mathbf{R}_j^{(\tau)})$ , otherwise b) kept with its weight set to unity. The bounds  $w_{min}$  and  $w_{max}$  are chosen to give a stable DMC walk with respect to the ensemble size and  $W_{tot}$ .

As discussed previously, incorporation of the normalization factor of Eq. (4) into  $\tilde{\kappa}(\tau)$  results in a decay independent of the reference energy  $E_{ref}$ . Therefore we are free to choose and vary  $E_{ref}$  based on considerations of numerical stability. A common choice of  $E_{ref}$  is the variational energy of the trial function,  $E_{ref} = \langle \Psi_T | \hat{H} | \Psi_T \rangle / \langle \Psi_T | \Psi_T \rangle$ , which may be obtained from a separate VMC calculation. One may also choose the ground state energy  $E_{ref} = E_0$ , which is readily obtained from standard ground state DMC methods. In our implementation, we begin with an initial choice of  $E_{ref}$  and update  $E_{ref}$  continuously during the course of the DMC walk according to

$$E_{ref}^{(\tau+\Delta\tau)} = E_{ref}^{(\tau)} + \frac{\eta}{\Delta\tau} \ln \left[ \frac{\sum_j w(\mathbf{R}_j^{(\tau)})}{\sum_j w(\mathbf{R}_j^{(\tau+\Delta\tau)})} \right] \quad (14)$$

where  $\eta$  is an empirical update parameter chosen to be as small as possible to avoid biasing the results, typically  $\eta/\Delta\tau = 0.01 - 0.3$ . The effect of this updating procedure for  $E_{ref}$  is to keep the average walker weight close to unity, thus preventing the ensemble size and sum of weights from diverging off to infinity or zero. The combination of these various mechanisms serve to ensure a stable DMC walk for long times, thus allowing the evaluation of small energy differences  $E_n - E_0$ . In the examples presented in Sec. 3 we will compare the effects of the various DMC schemes described here.

A final note in the implementation concerns the statistical errors in the excited state energy differences  $E_n - E_0$ . The MEM inversion of  $\tilde{\kappa}(\tau)$  gives the spectral function  $\kappa(E)$ , whose peak positions correspond to excited state energy differences. There is no general approach to assign error bars in the

mean peak position,<sup>2</sup> and thus we only report energies to the last significant figure. We determine empirically the position of this last significant figure by examining the convergence of  $E_n - E_0$  with respect to the number of decays  $\tilde{\kappa}(\tau)$  used as input for the MEM inversion. Because multiple projectors are usually sampled from the same DMC sidewalk, the *relative* differences between excited states are expected to be very accurate.

### 3 Examples

#### 3.1 $\text{NH}_3$ inversion

The first application we discuss here is a POITSE study of the ammonia inversion mode. Freezing all other internal degrees of freedom, the Schrödinger equation for this mode alone is a one-dimensional problem which can be solved exactly by a straightforward Discrete Variable Representation–Finite Basis Representation (DVR–FBR) calculation.<sup>11</sup> The Hamiltonian is given by

$$\hat{H} = -\frac{\hbar^2}{2\mu} \frac{\partial^2}{\partial h^2} + V(h), \quad (15)$$

where  $h$  is the distance between the nitrogen atom and the hydrogen plane,  $\mu$  is the effective mass for the mode and  $V(h)$  is the double-well inversion potential for tunneling across the hydrogen plane. We use one of the potential forms (“Case b”) proposed by Niño *et al.*<sup>12</sup> which leads to a tunneling splitting of  $1.43 \text{ cm}^{-1}$  for the lowest tunneling pair, and  $64.5 \text{ cm}^{-1}$  for the next lowest tunneling pair. The corresponding DVR–FBR energy levels are listed in Table 1 as benchmarks for the POITSE results.

A double well study was previously made in Ref. 2 to demonstrate the effectiveness of the POITSE method for model systems. However, in that example, the energy differences involved were much larger than those arising in the  $\text{NH}_3$  inversion problem which we discuss here. While the inversion frequency is high ( $993 \text{ cm}^{-1}$ ), the POITSE method allows the computation of an energy difference which is three orders of magnitude smaller. We compare here two different DMC implementations, namely pure weights and pure branching, and demonstrate the limitations associated with the former approach for

Table 1. Lowest four energy levels (in  $\text{cm}^{-1}$ ) for the inversion mode of  $\text{NH}_3$  relative to the ground state energy, which is  $553.11 \text{ cm}^{-1}$  above the potential minimum.

	$E_0$	$E_1$	$E_2$	$E_3$
DVR–FBR	0.00	1.43	961.40	1025.93

computing small energy differences. In order to make such a comparison of implementations, it is convenient and indeed preferable to use a system for which exact wave functions can be found.

The trial function  $\Psi_T(h)$  used in the Monte Carlo evaluation of Eq. (5) was initially fit to the DVR–FBR ground state eigenfunction  $\Phi_0(h)$ , and then further optimized by VMC. While numerous sophisticated VMC optimization schemes exist,<sup>13,14,15</sup> for a simple one-dimensional problem we found it sufficient to manually vary the trial function parameters to minimize the ground state energy and its variance. We use the analytical form

$$\Psi_T(h) = \exp[a_0 e^{b_0(h-c_0)^2} + a_0 e^{b_0(h+c_0)^2} + d_0 e^{e_0 h^4}], \quad (16)$$

where  $a_0, b_0, c_0, d_0$ , and  $e_0$  are parameters listed in Table 2. The corresponding VMC energy is  $561.4(3) \text{ cm}^{-1}$ , which is less than 2% above the exact ground state value obtained from DVR–FBR.

Since the first excited state  $\Phi_1(h)$  of a double well potential is the lowest antisymmetric state, the projector  $\hat{A} = h$  was previously used<sup>2</sup> to access this level. In obtaining higher-lying states, choosing  $\hat{A}$  to be an integer power of  $h$  led to a  $\tilde{\kappa}(\tau)$  consisting of a superposition of multiple exponential decays. For instance, a choice of  $\hat{A}\Psi_T(h) = h^2\Psi_T(h)$  resulted in non-negligible overlap with multiple excited levels. Thus an accurate Laplace inversion of the corresponding  $\tilde{\kappa}(\tau)$  was more difficult, due to the multiple decay contributions of these states. We use here instead more effective projectors given by the ratio of the eigenfunctions

$$\hat{A}_n = \frac{\Phi_n(h)}{\Psi_T(h)}, \quad (17)$$

where  $\Phi_n(h)$  is an excited state eigenfunction obtained from a DVR–FBR calculation. Clearly if the eigenfunctions are numerically exact, this results in an exact projector. Such projectors have also been shown to be useful when only symmetry properties of the eigenfunctions are well characterized.<sup>4</sup> The following analytical expressions were fitted to the DVR–FBR eigenfunctions for the lowest three excited states ( $n = 1 - 3$ ):

$$\Phi_1(h) = e^{b_1(h-c_1)^2} - e^{b_1(h+c_1)^2} \quad (18)$$

$$\Phi_2(h) = a_2[(h-f_2)e^{b_2(h-c_2)^2} - (h+f_2)e^{b_2(h+c_2)^2}] + d_2 e^{e_2 h^4} \quad (19)$$

$$\Phi_3(h) = a_3[(h-f_3)e^{b_3(h-c_3)^2} + (h+f_3)e^{b_3(h+c_3)^2}] + d_3 h e^{e_3 h^4}. \quad (20)$$

The fit parameters are given in Table 2. We emphasize that we are using this example of ammonia inversion to demonstrate and compare the relative

Table 2. Fit parameters (in atomic units) for NH<sub>3</sub> eigenfunctions obtained from DVR–FBR.

$n$	$a_n$	$b_n$	$c_n$	$d_n$	$e_n$	$f_n$
0	17.0	-1.095	0.829	1.	-0.054	
1		-10.886	0.681			
2	0.785	-11.072	0.674	-0.0664	-0.082	0.580
3	0.768	-12.025	0.720	-0.314	-1.325	0.447

efficiency of two different and alternative implementations of the POITSE algorithm. In particular, we shall compare the extent of noise and time step bias of the two different approaches to the DMC evaluation of Eq. (5). Our aim here is not to establish the generality of the method, or its accuracy for a double well problem, both of which have been addressed in earlier work.<sup>1,2</sup> Instead, we are interested in assessing the relative efficiency of different implementations, and thus it is preferable here to use projectors which are as exact as possible.

Since the lowest tunneling splitting  $E_1 - E_0$  is small, the corresponding decay  $\tilde{\kappa}(\tau)$  is slow and requires a long DMC propagation. Fig. 1a shows four typical  $\tilde{\kappa}(\tau)$ 's computed using the original POITSE implementation involving DMC with pure weights. These decays become extremely noisy as the time  $\tau$  increases. The ensemble local energy  $\langle E_L \rangle$  also exhibits such behavior. This problem is well-known<sup>8</sup> and arises from the fact that for long

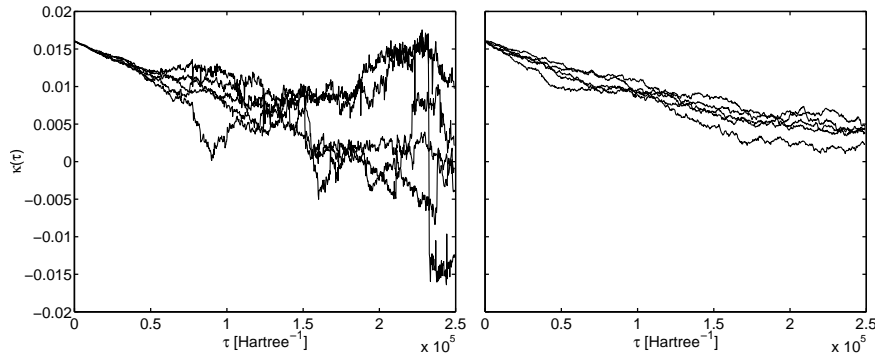


Figure 1. Typical correlation functions  $\tilde{\kappa}(\tau)$  for NH<sub>3</sub> using the projector  $\Phi_1/\Psi_T$ . The left plot (a) corresponds  $\tilde{\kappa}(\tau)$  evaluated using DMC with pure weights, while the decay curves in the right plot (b) are obtained using DMC with pure branching.

or even moderate DMC propagation times, the Monte Carlo ensemble averages are dominated by only a few walkers carrying high relative weights. In comparison, Fig. 1b shows typical  $\tilde{\kappa}(\tau)$ 's obtained from an implementation using DMC sidewalks with pure branching, where walkers are replicated or destroyed at each time step based on integer rounding of their weights as discussed in Sec. 2.2. In both calculations, 2000 walkers were propagated using a time step  $\Delta\tau$  of 5 Hartree<sup>-1</sup>. Clearly there is far less noise at longer times in the pure branching implementation, and thus such an approach is more suitable for the evaluation of small energy differences. Using the pure branching scheme, the Laplace inversion of 600 decays computed up to a final time  $\tau_f$  of 250000 Hartree<sup>-1</sup> results in a single peak at 1.39 cm<sup>-1</sup>, in reasonable agreement with the DVR-FBR value.

The evaluation of the larger energy differences  $E_2 - E_0$  and  $E_3 - E_0$  are manageable using both DMC implementations, because the lengths of the corresponding decays are much shorter than for the lowest energy difference  $E_1 - E_0$ . The use of the projector given in Eq. (17) facilitates the Laplace inversion, since each choice of  $\hat{A}_n$  results in a  $\tilde{\kappa}(\tau)$  consisting of only one exponential decay. In these calculations, 1000 decays are used as input for the MEM inversion, with each decay computed using an ensemble of 2000 DMC walkers propagated to a final time  $\tau_f$  of 1500 Hartree<sup>-1</sup>. The number of decays required for a converged  $\kappa(E)$  depends on the energy difference of interest and on the time step  $\Delta\tau$ . In general, for larger time steps, DMC with pure weights requires more sampling to produce fully converged results.

Since DMC methods are subject to a systematic time step bias, we perform a comparative study of the two implementations and their time step dependence. For the computation of the lowest energy difference  $E_1 - E_0$  using DMC with pure branching, we find a time step of 5 Hartree<sup>-1</sup> to be sufficiently small to give an accurate result within statistical error. However, the time step dependence of higher energy differences is not necessarily the same as that for  $E_1 - E_0$ . Fig. 2 presents the time step dependence for the calculation of  $E_2 - E_0$  and  $E_3 - E_0$ , using both DMC with pure weights (solid circles) and DMC with pure branching (open diamonds). It is evident that for both DMC implementations, the higher energy differences are more sensitive to time step bias than the lowest energy difference,  $E_1 - E_0$ . Thus, in order to extract the correct energies in the higher energy range, either a smaller time step would need to be used, or an extrapolation to  $\Delta\tau = 0$  would need to be performed.

With this simple example, we have shown that two different POITSE implementations, namely DMC with pure weights and DMC with pure branching, lead to the same results. We have also presented a systematic study of the

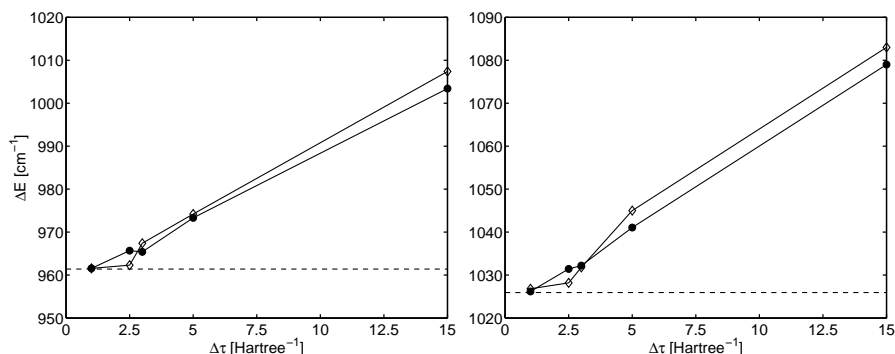


Figure 2. Time step dependence for the energy differences  $E_2 - E_0$  (left) and  $E_3 - E_0$  (right) of  $\text{NH}_3$  inversion mode. The dashed lines correspond to the exact DVR-FBR values. Energies obtained from DMC with pure weights are marked with filled circles, and energies obtained from DMC with pure branching are marked with open diamonds.

convergence behavior for these two different approaches, and compared with the exact solution obtained from DVR-FBR calculations. For the evaluation of small energy differences, we conclude that a pure branching DMC sidewalk is considerably more efficient than using DMC with pure weights.

### 3.2 $^4\text{He}$ -benzene dimer

We now demonstrate the use of the POITSE approach for the computation of excited vibrational energies of the  $^4\text{He}$ -benzene dimer. We treat the benzene as a rigid molecule, and for simplicity we also neglect the rotational kinetic energy of the benzene, *i.e.* the rotation of benzene relative to helium. In the space-fixed frame, the resulting Hamiltonian is

$$\hat{H} = -\frac{\hbar^2}{2m_0}\nabla_0^2 - \frac{\hbar^2}{2m}\nabla_k^2 + V(\mathbf{r}), \quad (21)$$

where  $m_0$  is the benzene mass,  $m$  is the helium mass,  $\nabla_0^2$  is the Laplacian with respect to the benzene center-of-mass position  $\mathbf{r}_0$ ,  $\nabla_k^2$  is the Laplacian with respect to the helium position  $\mathbf{r}_k$ , and  $V(\mathbf{r})$  is the  $^4\text{He}$ -benzene interaction potential. The latter depends only on the relative coordinate vector  $\mathbf{r} = \mathbf{r}_k - \mathbf{r}_0$ . The potential is an analytical fit<sup>16</sup> to *ab initio* MP2 calculations of Hobza *et al.*,<sup>17</sup> and possesses two equivalent global minima of  $-66.01 \text{ cm}^{-1}$  along the six-fold  $C_6$ -axis, situated at  $3.27 \text{ \AA}$  above and below the benzene

plane. While in principle one could transform the Hamiltonian to the center-of-mass frame to yield a three-dimensional problem, as would typically be done in a basis set calculation, sampling the transformed kinetic energy terms becomes more complicated in DMC as additional particles are added, and thus it is technically simpler for us to work with the six-dimensional Hamiltonian as written in Eq. (21).

The trial function  $\Psi_T(\mathbf{r})$  is the product of an anisotropic Gaussian binding factor centered on the benzene center-of-mass, and an atom-atom repulsive factor,

$$\Psi_T(\mathbf{r}) = e^{-a(x^2+y^2)-cz^2} \prod_{\alpha} e^{t_{\alpha}(r_{\alpha})} \prod_{\beta} e^{t_{\beta}(r_{\beta})}, \quad (22)$$

where we use for the binding parameters (in atomic units)  $a = 0.05$ ,  $c = 0.06$ . The product over  $\alpha$  and  $\beta$  runs over the carbon atoms and hydrogen atoms, respectively. The atom-atom terms  $t_{\alpha}(r_{\alpha})$  and  $t_{\beta}(r_{\beta})$  are functions of  ${}^4\text{He}$ -carbon and  ${}^4\text{He}$ -hydrogen distances  $r_{\alpha}$  and  $r_{\beta}$  respectively, and their analytical forms are chosen to cancel out the leading singularities in the atom-atom potential energy terms.<sup>18</sup> In this study we use  $t_{\alpha}(r_{\alpha}) = -c_{\alpha}r_{\alpha}^{-6}$ ,  $t_{\beta}(r_{\beta}) = -c_{\beta}r_{\beta}^{-5}$ , with the parameters (in atomic units)  $c_{\alpha} = 6000$ ,  $c_{\beta} = 8000$ . The trial function of Eq. (22) possesses the same  $D_{6h}$  symmetry as the  ${}^4\text{He}$ -benzene potential.

A ground state DMC calculation using the trial function and potential discussed above gives a ground state energy  $E_0 = -21.61(2) \text{ cm}^{-1}$ , which corresponds to about 32% of the global energy minimum of the  ${}^4\text{He}$ -benzene potential. Such a high zero-point energy is typical of helium van der Waals systems,<sup>19</sup> and underscores the need for a fully quantum mechanical treatment of the van der Waals degrees of freedom.

We choose the excitation operators  $\hat{A}^{(\Gamma)}$  based on symmetry considerations, where the superscript  $\Gamma$  denotes an irreducible representation of the  $D_{6h}$  point group. Since the trial function  $\Psi_T(\mathbf{r})$  transforms as the totally symmetric representation  $A_{1g}$ , for a given  $\hat{A}^{(\Gamma)}$ , the integral  $\langle \Psi_T | \hat{A}^{(\Gamma)} | \phi_n \rangle$  in Eq. (8) is only nonzero for states  $|\phi_n\rangle$  which transform as  $\Gamma$ . Thus an appropriate choice of  $\hat{A}^{(\Gamma)}$  will, by symmetry, significantly reduce the number of terms in the summation of Eq. (8), leaving only decay terms whose characteristic decay times are presumably more well-separated, and thus easier to resolve. The various choices of the operators  $\hat{A}^{(\Gamma)}$  we use here are listed in Table 3, where  $\hat{A}^{(\Gamma)}$  is defined with respect to the benzene principal axis frame centered on the benzene center-of-mass. In this coordinate system, the  $x$ -axis is perpendicular to the benzene C-C bond, the  $y$ -axis lies along the benzene C-H bond, and the  $z$ -axis is perpendicular to the benzene plane.

Table 3. Operators  $\hat{A}^{(\Gamma)}$  and the resulting energies  $E - E_0$  (in  $\text{cm}^{-1}$ ) for  $^4\text{He}$ -benzene van der Waals excitations. For the two-dimensional irreducible representations, the two projectors listed give degenerate energies. The three rightmost columns list energies obtained from hybrid branching/weighting (B/W), pure weighting (PW), and pure branching (PB).

$\Gamma$	$\hat{A}^{(\Gamma)}$	$E - E_0$		
		B/W	PW	PB
$E_{1g}$	$xz, yz$	6.39	6.39	6.39
$E_{1u}$	$x, y$	7.04	6.97	7.04
$A_{2u}$	$z(x^2 + y^2)$	7.76	7.64	7.86
$A_{1g}$	$x^2 + y^2$	8.44	8.54	8.44
$E_{2u}$	$z(x^2 - y^2), xyz$	9.41	9.36	9.48
$E_{2g}$	$x^2 - y^2, xy$	9.96	9.84	10.01
$B_{2u}$	$x^3 - 3xy^2$	11.22	11.34	11.19
$B_{1g}$	$z(x^3 - 3xy^2)$	11.41	11.56	11.58
$B_{2g}$	$z(y^3 - 3x^2y)$	13.34	13.39	13.25
$B_{1u}$	$y^3 - 3x^2y$	13.58	13.58	13.37

To evaluate the correlation function  $\tilde{\kappa}(\tau)$ , we sample an initial ensemble of 1000 walkers from every 100 steps of a VMC walk. This initial ensemble is propagated by a DMC sidewalk with a time step of  $\Delta\tau = 10$  Hartree $^{-1}$ . In the  $^4\text{He}$ -benzene system, the energy differences of interest are sufficiently large such that we can employ and compare all three DMC implementations discussed in Sec. 2.2. For the hybrid branching/weighting scheme, the ensemble size and sum of weights in the DMC propagation are kept at approximately 1000 on average by choosing an appropriate set of DMC parameters  $w_{min}, w_{max}$ , and  $\eta$  (Eq. (14)). For DMC with pure weights and DMC with pure branching, the only adjustable parameter is the update parameter  $\eta$ . About 500 independent decays  $\tilde{\kappa}(\tau)$  are generated in this manner, and subsequently used as input for the MEM inversion, resulting in the spectral function  $\kappa(E)$ . Each choice of projector  $\hat{A}^{(\Gamma)}$  results in a single dominant peak in the corresponding  $\kappa(E)$ , and the peak positions are listed in Table 3. These excited state energies show general agreement (to within  $\sim 0.2$   $\text{cm}^{-1}$ ) between the three DMC implementations.

In Fig. 3 we superimpose the spectral functions obtained using the hybrid branching/weighting approach. There, the peaks are grouped in doublets whose splittings range from  $\sim 0.2 - 0.7$   $\text{cm}^{-1}$ . These doublets are due to projectors which are symmetric and antisymmetric with respect to reflection about the benzene plane. They constitute a tunneling splitting

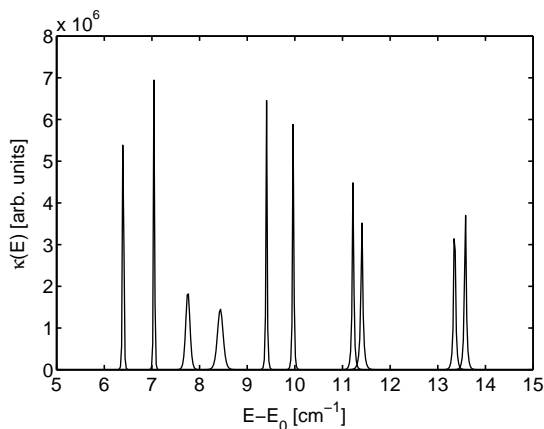


Figure 3. Spectral function  $\kappa(E)$  for  $^4\text{He}$ -benzene, computed using a hybrid branching/weighting approach. Note that this plot represents a superposition of  $\kappa(E)$ 's obtained from multiple projectors, each yielding a single peak from the MEM inversion.

between the two equivalent global potential minima along the benzene  $C_6$ -axis, above and below the aromatic ring plane. Tunneling of helium around a planar moiety has also been observed in basis set calculations for the 2,3-dimethylnaphthalene-He complex, where the magnitude of the splittings ranged from  $< 10^{-4} \text{ cm}^{-1}$  for localized states up to  $3.2 \text{ cm}^{-1}$  for highly delocalized states.<sup>20</sup> The tunneling splittings which we obtain here exhibit a decrease in magnitude with increasing energy. Since the energies of highest levels correspond to about 12% of the  $^4\text{He}$ -benzene potential energy minimum, this decrease in the tunneling splitting can be attributed to increasing anharmonicities in the  $^4\text{He}$ -benzene interaction potential as these levels approach dissociation. Inclusion of the benzene rotational kinetic energy term into the Hamiltonian of Eq. (21) qualitatively changes the features of the energy spectrum, removing this decrease in the tunnel splitting. The specific effects of this rotational contribution, as well as the general physics of  $^4\text{He}_N$ -benzene clusters, will be reported in a future study.<sup>21</sup>

#### 4 Conclusion

We have extended the applicability of the POITSE method by introducing branching processes in the DMC evaluation of an imaginary time correlation function  $\tilde{\kappa}(\tau)$ . The effects of branching were tested in the determination of

excited state energies for two simple systems, namely the one-dimensional ammonia inversion mode and the six-dimensional  $^4\text{He}$ -benzene van der Waals modes. While in an ideal situation one would employ a pure weighting scheme in the DMC propagation, in the ammonia study we were faced with the problem of evaluating a slowly decaying  $\tilde{\kappa}(\tau)$  corresponding to a small tunneling splitting. Thus, the incorporation of branching in the DMC sidewalk is essential for the stable computation of small energy differences. We have also provided a comparison between the various branching schemes and the pure weighting scheme in the  $^4\text{He}$ -benzene example, and have demonstrated that the results obtained are in good numerical agreement.

The incorporation of branching as described here has been critical in allowing excited state energies to now be evaluated for much larger systems using the POITSE approach.<sup>21,22</sup> Another current modification in progress includes the implementation of descendant weighting techniques<sup>23,9,24,25</sup> to construct an estimate of the exact ground state wave function  $|\phi_0\rangle$  “on-the-fly”. The projector  $\hat{A}$  would then operate on the exact  $|\phi_0\rangle$ , instead of an approximate trial function  $|\Psi_T\rangle$ . These improvements in the general POITSE methodology open the way for efficient and accurate Monte Carlo evaluation of excited state energies for large systems.

### Acknowledgments

Financial and computational support from the National Science Foundation through grant CHE-9616615. An allocation of supercomputing time from the National Partnership for Advanced Computational Infrastructure (NPACI) is gratefully acknowledged.

### References

1. D. Blume, M. Lewerenz, P. Niyaz, and K. B. Whaley, *Phys. Rev. E* **55**, 3664 (1997).
2. D. Blume, M. Lewerenz, and K. B. Whaley, *J. Chem. Phys.* **107**, 9067 (1997).
3. D. Blume, M. Mladenović, M. Lewerenz, and K. B. Whaley, *J. Chem. Phys.* **110**, 5789 (1999).
4. D. Blume and K. B. Whaley, *J. Chem. Phys.* **112**, 2218 (2000).
5. R. K. Bryan, *Eur. Biophys. J.* **18**, 165 (1990).
6. D. Blume, Ph.D. thesis, University of Göttingen, 1998.
7. B. L. Hammond, W. A. Lester, Jr., and P. J. Reynolds, *Monte Carlo Methods in Ab Initio Quantum Chemistry* (World Scientific, Singapore,

- 1994).
8. R. Assaraf, M. Caffarel, and A. Khelif, *Phys. Rev. E* **61**, 4566 (2000).
  9. R. N. Barnett, P. J. Reynolds, and W. A. Lester, Jr., *J. Comp. Phys.* **96**, 258 (1991).
  10. D. Blume, M. Lewerenz, F. Huisken, and M. Kaloudis, *J. Chem. Phys.* **105**, 8666 (1996).
  11. C. Leforestier, *J. Chem. Phys.* **94**, 6388 (1991).
  12. A. Niño and C. Muñoz-Caro, *Computers Chem.* **19**, 371 (1995).
  13. C. J. Umrigar, K. G. Wilson, and J. W. Wilkins, *Phys. Rev. Lett.* **60**, 1719 (1988).
  14. M. Snajdr and S. M. Rothstein, *J. Chem. Phys.* **112**, 4935 (2000).
  15. M. P. Nightingale and V. Melik-Alaverdian, see article in this volume.
  16. Y. Kwon and K. B. Whaley, *J. Chem. Phys.* **114**, 3163 (2001).
  17. P. Hobza, O. Bludský, H. L. Selzle, and E. W. Schlag, *J. Chem. Phys.* **97**, 335 (1992).
  18. A. Mushinski and M. P. Nightingale, *J. Chem. Phys.* **101**, 8831 (1994).
  19. K. B. Whaley, *Advances in Molecular Vibrations and Collision Dynamics* (JAI Press Inc., Greenwich, CT, 1998), p. 145.
  20. A. Bach, S. Leutwyler, D. Sabo, and Z. Bačić, *J. Chem. Phys.* **107**, 8781 (1997).
  21. P. Huang and K. B. Whaley, (2001), to be submitted to *Phys. Rev. B*.
  22. A. Viel and K. B. Whaley, *J. Chem. Phys.* (2001), submitted to *J. Chem. Phys.*
  23. K. S. Liu, M. H. Kalos, and G. V. Chester, *Phys. Rev. A* **10**, 303 (1974).
  24. J. Casulleras and J. Boronat, *Phys. Rev. B* **52**, 3654 (1995).
  25. M. Hornik, M. Snajdr, and S. M. Rothstein, *J. Chem. Phys.* **113**, 3496 (2000).